Reduction in Tactoid Size as a Means for Reinforcing High-Density Polyethylene/Montmorillonite Nanocomposites

Carla Marega,[1] Valerio Causin,[1] Antonio Marigo,[1] Giuseppe Ferrara[2]

[1]*Dipartimento di Scienze Chimiche, Università di Padova, and INSTM Research Unit, via Marzolo 1, Padova 35131, Italy*
[2]*LyondellBasell Poliolefine Italia SpA, Centro Ricerche 'Giulio Natta', P.le Donegani 12, Ferrara 44100, Italy*

Received 13 January 2009; accepted 15 March 2009
DOI 10.1002/app.30411
Published online 27 May 2009 in Wiley InterScience (www.interscience.wiley.com).

ABSTRACT: Nanocomposites were prepared by adding montmorillonite clay to a high-density polyethylene matrix. Their structure, morphology, thermal behavior, and physical– mechanical properties were studied. The filler did not alter much the structure and morphology of the matrix, with the exception of a disruptive effect on the lamellar stacks. The crystallization behavior, equilibrium melting temperature, and work of chain folding of the nanocomposites were also unaltered with respect to that of the PE base polymer. However, significant improvements in physical–mechanical properties were observed. The reason for this increase in performance was ascribed to the interaction between the filler and the matrix, especially because of a reduction in size of the original tactoids to stacks of just a few layers, albeit not intercalated. © 2009 Wiley Periodicals, Inc. J Appl Polym Sci 113: 3920–3928, 2009

Key words: nanocomposites; polyethylene; montmorillonite; clay; small and wide angle x-ray scattering

INTRODUCTION

In the last few years, polymer-layered silicate nanocomposites have attracted a vast research activity, because of the promise of large property improvements with the addition of very small quantities of nanometer-sized fillers.[1] Montmorillonite (MMT) is probably the most commonly used clay for the preparation of these materials. To obtain the expected performance, the degree of interaction between matrix and filler is critical. A phase-separated structure, resembling that of traditional microcomposites, can be obtained when polymer and clay do not interact; an intercalated morphology is observed when macromolecular chains penetrate inside the clay layers; an exfoliated structure is attained when single clay sheets are delaminated and dispersed in the matrix. The nanometric dispersion associated to intercalation and exfoliation increases the aspect ratio of clay platelets, maximizes the interfacial region between filler and matrix, and consequently reinforces the material. Only a fraction of the hundreds of articles on polymer-layered silicate nanocomposites is on high-density polyethylene (HDPE),[2–20] despite the very relevant technological and commercial importance of this material. The study of the crystallization behavior of HDPE-clay nanocomposites is especially underrepresented. Xu et al.[21–23] investigated the crystallization of a linear PE synthesized by polymerization of ethylene with a metallocene catalyst intercalated within MMT layers. They observed that clay exerts a double role in nonisothermal crystallization: on one hand, it restricts the mobility of the chains and on the other hand, it acts as a nucleating agent. These effects are reflected by the appearance of an induction period and by a faster overall crystallization rate in the case of the intercalated sample with respect to exfoliated ones.[23] In the case of isothermal crystallization, intercalation of PE within clay layers brought about a slower crystallization rate, with 2D growth.[22] Confined PE crystals had a lower melting temperature.[22] These authors also showed that at a high content of clay, the mobility of the polymer chains can be reduced to such an extent that the relative rates of secondary nucleation and surface spreading are changed and Regime III crystallization can be clearly observed.[21] It should be remarked that the transition between Regimes II and III is normally quite difficult to measure, because rapid cooling or other techniques must be used.[21] Yuan et al.[14] studied the nonisothermal crystallization behavior of HDPE-clay nanocomposites, comparing it with analogous PP-based materials. They concluded that HDPE is less sensitive to the

Correspondence to: V. Causin (valerio.causin@unipd.it).

nucleating effect of clay than PP. They found that the nucleating effect of clay was decreased if the mobility of polymer chains decreased, i.e. if they were confined within the filler. They also noted a decrease in crystallinity degree with increasing filler content.[14] Gopakumar et al.[3] and Chaiko[15] found that clay promotes nucleation, on the contrary Osman and Atallah[5] reported that organo-MMT does not nucleate crystallization of HDPE under slow cooling conditions. Another yet controversial issue is the effect of clay on HDPE physical–mechanical properties. Some authors reported significant improvements, especially in modulus,[11,12] usually although with a concurrent decrease in impact strength.[7,9,10] Impact strength could be retained in the composites with respect to the neat matrix, at the expense of a more marginal increase in modulus[13,18] and in an instance an increase in Izod impact strength was reported by Liang et al.[4] Other authors obtained only limited improvements in physical–mechanical properties.[6,8,17,19] Mainil et al. pointed out that a key factor that influences the performance, and especially the modulus, of these materials is the compatibilization of the matrix. In this article, we report the structural, morphological, and physical–mechanical characterization of nanocomposites prepared using a novel compatibilizer, a low-density copolymer of polyethylene, acrylic acid, and butyl acrylate. The isothermal crystallization behavior of such materials is studied, also with a measure of the thermodynamic melting temperature. Wide angle x-ray diffraction (WAXD), small angle x-ray scattering (SAXS), differential scanning calorimetry (DSC) and polarized light optical microscopy (PLOM) were used to characterize the samples.

EXPERIMENTAL

Samples and sample preparation

For the preparation of the composites, the matrix used consisted of HDPE Lupolen 4261AG (LyondellBasell Polyolefins), with density of 0.945 g/cm^3, and melt flow rate (MFR) of 6 g/10 min (ASTM D 1238, 190°C, 21.6 kg). The compatibilizer was Lucalen A2920M (LyondellBasell Polyolefins), a low-density polyethylene with density of 0.927 g/cm^3, MFR of 7 g/10 min (ASTM D 1238, 190°C, 2.16 kg). In Lucalen, ethylene was copolymerized with acrylic acid (4%) and butyl acrylate (7%). Cloisite 15A, an organomodified MMT was used as a filler. Table I shows the composition of the considered samples. The samples were denominated by PE followed by a number that represents the percentage of added clay. All the nanocomposites were prepared on a Leistritz Micro 27 twin-screw extruder, equipped with gravimetric feeders. The line is composed of 10 barrels for a total

TABLE I
Composition, Physical–Mechanical Characterization and Thermal Degradation Data of the Samples

	Lucalen (%)	Clay (%)	MEF (N/mm^2)	Izod at 23°C (kJ/m^2)	Stress at yield (N/mm^2)	Strain at yield %	Stress at break (N/mm^2)	Strain at break (%)	Vicat (°C)	Full notch creep test (h)	$T_{onser}^{deg,rad}$ (°C)	$T_{max}^{deg,rad}$ (°C)	$T_{offset}^{deg,rad}$ (°C)
PE	0	0	870	103	22	12	21	155	127	45	454	480	491
PE05	0.5	0.5	875	86	24	15	22	105	127	43	441	464	475
PE1	1	1	923	91	24	16	22	95	127	52	445	461	471
PE2	2	2	932	98	25	16	22	70	127	48	444	459	468
PE5	5	5	1012	99	25	16	23	50	127	139	440	459	464

MEF = Flexural Elastic Modulus.

of 40 L/D. All components were fed through first feeding port, nitrogen was fed to main port and vacuum degassing was applied on Barrel 9. Strand cutting was then applied. Processing conditions used were capacity = 7 kg/h; screw speed = 200 rpm; torque level = 87–92%; barrel temperature set point = 200°C and melt temperature = ~245°C.

Wide angle x-ray diffraction

WAXD patterns were recorded in the diffraction angular range 1.5°–50° 2θ by a Philips X'Pert PRO diffractometer, working in the reflection geometry and equipped with a graphite monochromator on the diffracted beam (CuK_α radiation). Transmission patterns were also recorded in the diffraction range 10°–50° 2θ by a diffractometer GD 2000 (Ital Structures) working in a Seeman-Bohlin geometry and with a quartz crystal monochromator on the primary beam ($CuK_{\alpha 1}$ radiation). The application of the least-squares fit procedure elaborated by Hindeleh and Johnson[24] gave the degree of crystallinity by weight (X_{WAXD}).

Small angle x-ray scattering

The SAXS patterns of the samples were recorded by an MBraun system, using CuK_α radiation from a Philips PW 1830 X-ray generator. The data were collected by a position sensitive detector in the scattering angular range 0.1°–5.0° 2θ, and they were successively corrected for blank scattering.

A constant continuous background scattering was then subtracted[25] and the obtained intensity values $\tilde{I}(s)$ were smoothed in the tail region, with the aid of the $s\tilde{I}(s)$ vs. $1/s^2$ plot.[26]

Finally, the Vonk's[27] desmearing procedure was applied and the one-dimensional scattering function was obtained by the Lorentz correction $I_1(s) = 4\pi s^2 I(s)$, where $I_1(s)$ is the one-dimensional scattering function and $I(s)$ the desmeared intensity function, being $s = (2/\lambda) \sin \theta$.

SAXS data analysis

A fitting method of SAXS patterns was developed on the basis of a theoretical model[28–31] in which the clay structure is represented by high-density clay layers alternated by low-density matter, either polymer or compatibilizing agent. The lateral width of the clay stacks was assumed to be much larger than its thickness,[32] so a one-dimensional variation was considered for electron density.[33]

The intensity profile was evaluated as:

$$I(s) = I^{\mathrm{I}}(s) + I^{\mathrm{II}}(s) \tag{1}$$

where:

$$I^{\mathrm{I}}(s) = \frac{(\rho_Y - \rho_Z)^2}{4\pi^2 s^2 D} \times \frac{|1 - F_Y|^2\left(1 - |F_Z|^2\right) + |1 - F_Z|^2\left(1 - |F_Y|^2\right)}{(1 - F_Y F_Z)^2} \tag{2}$$

$$I^{\mathrm{II}}(s) = \frac{(\rho_Y - \rho_Z)^2}{2\pi^2 s^2 DN} \times \mathrm{Re}\left\{\frac{F_Z(1 - F_Y)^2\left(1 - (F_Y F_Z)^N\right)}{(1 - F_Y F_Z)^2}\right\} \tag{3}$$

In these equations, F_Y and F_Z represent the Fourier transforms of the distribution functions of the clay layers (Y) and of the low-density regions interposed between the clay platelets (Z), ρ_Y and ρ_Z are the electron densities of the clay and low-density regions, respectively, N is the number of layers and X is the average long period. The thickness Y of the alumino-silicatic layers was fixed at 1.0 nm.[34]

Polarized light optical microscopy

The spherulitic morphology of the samples was studied with a Leica DM4000M polarized light microscope. The pellets obtained by extrusion were placed between a microscope glass slide and a cover slip in an oven preset at 160°C for 15 min, to ensure uniform melting and to delete their thermal history. Subsequently, the samples were transferred to a Mettler FP82HT hot stage and isothermally crystallized at 124°C. The photomicrographs were taken between crosspolarizers with a Leica DFC280 digital camera after the crystallization was completed, i.e., when no further change in the spherulites appearance could be noted.

Differential scanning calorimetry

All the measurements were carried out with a TA Instruments mod. 2920 calorimeter operating under N_2 atmosphere. Polymer samples weighing about 5 mg closed in aluminum pans were used throughout the experiments. Indium and tin of high purity were used for calibrating the DSC temperature and enthalpy scales.

A heating rate of 10°C/min up to 160°C was set to observe the polymer melting peak. After erasure of thermal history by a 5 min isotherm at 160°C, the sample was cooled down to room temperature at 10°C/min and heated again to 160°C at the same rate.

The T_m^0 of the samples was determined by the technique proposed by Marand and coworkers.[35–37] After erasure of thermal history at 160°C for 5 min, samples were rapidly brought to the desired T_c and

allowed to crystallize for a time t_c, and subsequently heated to 160°C at 10°C/min. The instrumental drift associated to the rapid jump toward crystallization temperature (T_c) was estimated by running a DSC experiment with an inert Al_2O_3 sample of the same mass (5 mg) as that used for polymer samples. Crystallization temperatures were chosen so that the induction time before the beginning of crystallization was larger than the time requested by the apparatus to recover from the instrumental drift.

The peak maximum of the melting endotherm was taken as the melting point. For each T_c, crystallization was repeated for six or seven different t_c's, using the same sample to avoid the effect of sample preparation. A prior evaluation of resistance to thermal degradation was made according to Juhász et al.[37] By TGA experiments, performed on a TA Instruments SDT 2960 apparatus, it was checked that the onset of degradation was located beyond 160°C. It was possible to obtain the melting temperature of initial and nonthickened lamellae, T_m, by extrapolation to the induction time t_0. t_0 has been evaluated as the time when the first deviation of the thermogram baseline is detected. Variables $X = T_m^0/(T_m^0 - T_c)$ and $M = T_m^0/(T_m^0 - T_m)$ were thus evaluated with tentative T_m^0 values, and each time a M vs. X plot was drawn to verify the following expression[35]:

$$M = \gamma(X + a) \tag{4}$$

γ is the thickening coefficient, which tends to 1 in the absence of thickening phenomena, i.e., at the beginning of crystallization. a is a dimensionless term that accounts for the nonlinearity of $T_m - T_c$ data.

The kinetics of crystallization was studied by subjecting each sample to the following thermal cycle: after erasure of previous thermal history by keeping the polymer at 160°C for 5 min, it was cooled at the maximum rate to the crystallization temperature (T_c). The heat evolved during the transition was monitored as a function of time during an isothermal at T_c of suitable length. The fraction X_c of material crystallized after the time t was estimated from the relation:

$$X_c = \int_0^t \left(\frac{dH}{dt}\right) dt \Big/ \int_0^\infty \left(\frac{dH}{dt}\right) dt \tag{5}$$

where the numerator is the heat generated at time t and the denominator is the total heat of crystallization. The Avrami equation[38–40] was used to correlate X_c with time:

$$X_c = 1 - \exp[-K(t - t_0)^n] \tag{6}$$

K is the kinetic constant of crystallization, n is a coefficient linked to the time dependence and the dimensions of growth of crystallites.

The crystallization behavior of the polymer was also studied according to the relationship between chain folded crystal growth rate and undercooling proposed by Lauritzen and Hoffman[41]:

$$\ln G + \frac{U^*}{R(T_c - T_\infty)} = \ln G_0 - \frac{K_g}{T_c \Delta T f} \tag{7}$$

where G is the crystal growth rate, U^* is a constant characteristic of the activation energy for chain motion and is equal to 1500 cal/mol, R is the gas constant, $T_\infty = T_g - 30$, T_g being the glass transition temperature, f is a correction factor equal to $2T_c/(T_m + T_c)$ and G_0 is a preexponential factor.

The constant K_g is given by:

$$K_g = \frac{jT_m^0 b_0 \sigma \sigma_e}{k\Delta H} \tag{8}$$

where j is an integer equal to 2 in the second regime of crystallization and to 4 in the first and third regime of crystallization, b_0 is the thickness of the surface layer, σ and σ_e are the interfacial free energies of the lateral and fold surface, respectively, k is the Boltzmann constant, and ΔH is the enthalpy of fusion per mole of repeat units.

Physical–mechanical properties

The specimens for mechanical testing and for WAXD and SAXS analyses were prepared in accordance with ISO 294 and conditioned for 40 h at 23°C ± 2°C and 50% ± 5% relative humidity following ISO 291. The flexural and elongational properties were determined in accordance with ISO 178 using a Model 4301 instrument (Instron) on injection-molded specimens, prepared after ISO 294-1. Impact strength was measured with a 6545 pendulum-type hammer (Ceast) striking a notched specimen with a 0.05 mm notch (ISO 180). Heat deflection temperature was evaluated with a CEAST HDT6 placing the specimen in an oil bath under a load of 460 kPa (ISO 75).

Thermogravimetry

Thermogravimetric analysis (TGA) was performed with a SDT 2960 simultaneous TG/DSC system (TA Instruments). The scans were recorded at a heating rate of 20°C/min in a temperature range from 30 to 700°C. Experiments were done in nitrogen atmosphere.

RESULTS AND DISCUSSION

The structure and morphology of the samples were characterized by WAXD and SAXS. Figure 1 shows the obtained WAXD patterns. A variation of relative peak intensities is evident, with the (200) signal

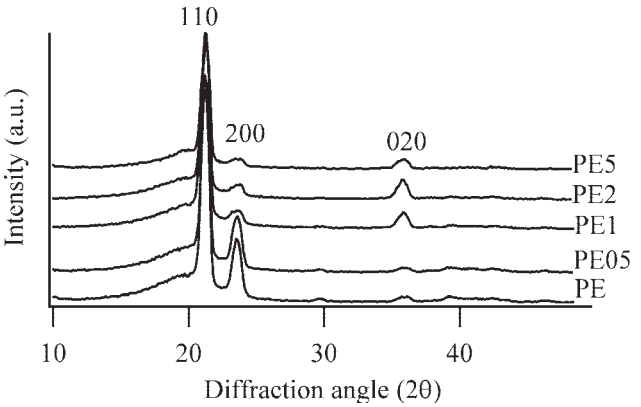

Figure 1 WAXD patterns of the considered samples. The indices of the main peaks are indicated.

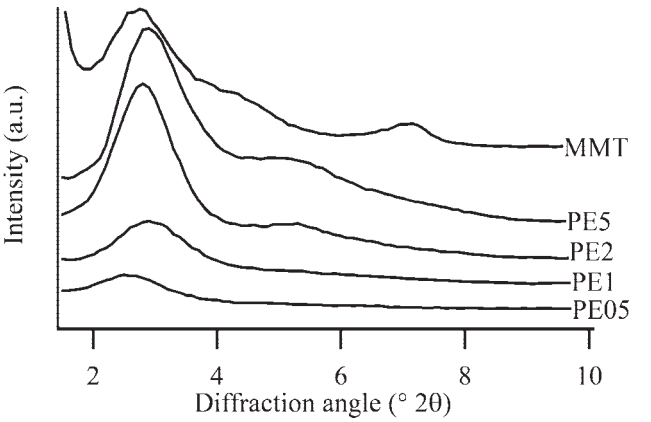

Figure 3 WAXD patterns of the composite samples and of pristine montmorillonite in the clay tactoids' periodicity region.

decreasing as a function of clay content, whereas the (020) intensity increases with the filler percentage. This should be associated to a preferential orientation of the polymer due to the presence of clay layers.[3,20] The crystallinity degree of the materials was measured by WAXD. No significant variation was found among the samples: all of them displayed a crystallinity of 57% ± 1%. The effect of clay on the semicrystalline framework of PE has not been cleared yet. Many authors report a variation of crystallinity as a consequence of the addition of filler, either an increase[13,17] or a decrease.[3,4,10,14] In other instances, such as in this study, the crystallinity remained unaltered.[5–7,42] In the absence of variations in the degree of crystallinity in their nanocomposites, the observed improvements in properties were ascribed in the literature to modifications of the polymer lamellar morphology[13,42,43] or entirely to the action of the filler.[5–7,11,13] The polymer lamellar morphology was studied in this work by SAXS. Figure 2 shows the obtained patterns. As may be seen, the signal due to lamellar stacks progressively weakens and disappears with increasing filler content, confirming the disrupting role of clay on the lamellar morphology.[11,44–47]

The dispersion of clay in the matrix was also characterized. Figures 3 and 4 show the WAXD and SAXS patterns relative to the angular range typical of the clay basal peaks. No significant shift of the (001) signal of MMT could be observed, between the composite samples and also with respect to the basal peak of the neat filler used in this work (Fig. 3). Difficulties in intercalating clay layers with HDPE chains are well known.[10,11,16,48,49] The peaks due to the stacked clay were fit to obtain the average number of layers in each tactoid. The crystallite size (L_{001}) of the tactoids was estimated by the Scherrer equation:[32] dividing L_{001} by the periodicity d_{001} of the basal peak, the number of layers N_{WAXD} could be assessed. For all the nanocomposites, N_{WAXD} was equal to two layers per tactoid. Verification of this datum was sought by fitting the SAXS patterns according to theoretical models.[28,30,31] Only the sample containing 5% filler yielded a SAXS peak intense enough to be fitted. By this procedure, it resulted that clay stacks in sample PE5 have an average number of layers of three, substantially confirming WAXD results. Moreover, this also excludes the

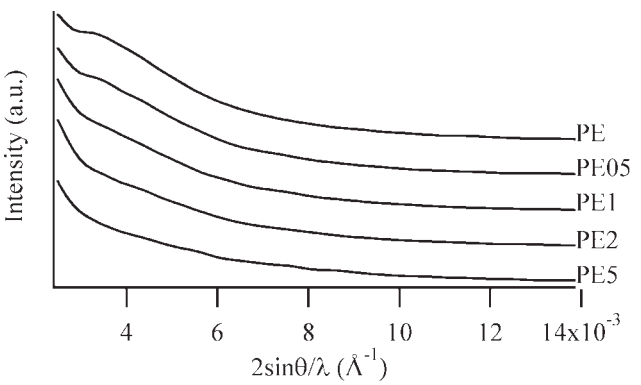

Figure 2 SAXS pattern of the samples in the polymer lamellar periodicity region.

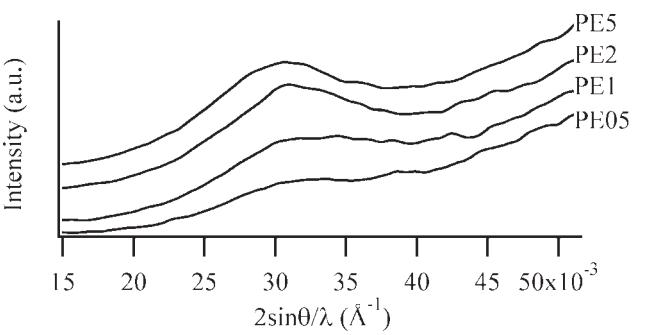

Figure 4 SAXS pattern of the composite samples in the clay tactoids' periodicity region.

existence of face-to-face aggregation, which can be detected by SAXS, but not by WAXD.[31] The width and low intensity of the clay peaks in the SAXS patterns of the samples containing less filler are indicative of very small tactoids; therefore, substantiating the information obtained by the Scherrer equation. Pristine MMT aggregates have therefore broken down into much smaller stacks.[2,12] This situation, for the purpose of property enhancement, can be considered equal to an exfoliated dispersion of individual layers.[46,47,50] Indeed, an improvement in physical–mechanical properties was achieved. As can be seen in Table I, nanocomposites had higher modulus and properties at yield than the matrix, and retained most of the pristine impact strength, stress at break, and softening point as measured by vicat. The increase in yield properties and modulus should also be ascribed to an effect of the compatibilizer.[16] Modulus increased more rapidly beyond a threshold quantity of filler, about 1%. A similar behavior was found for example in EPR/MMT nanocomposites.[46] An increase in the surface area of interaction between polymer and filler, as in the case of exfoliated or intercalated systems, is associated to the increase of the modulus of the material,[51,52] because the hindering to the mobility of the chains is maximized. Sample PE5 showed a good mechanical performance, especially a large increase in the full notch creep test. Creep behavior is controlled by the deformation of the amorphous phase.[11] Impact strength is moreover negatively influenced by the presence of crystalline material at the polymer–filler interface.[13] The relatively high quantity of filler contained in PE5 determined a thorough disruption of the semicrystalline framework, greatly improving the creep behavior and resistance to impact. The decrease in the strain at break is a common feature in clay containing nanocomposites, because of the confinement of the molecules between MMT layers.

The thermal stability of the composites was probed by TGA. In accord with the literature,[8,9,53] a slightly anticipated degradation (Table I) was observed in inert atmosphere, probably due to the catalytic effect that clay exerts toward the degradation of the PE matrix.[9,53]

The thermal properties of the samples were studied by DSC. As described in the experimental section, all the samples were subjected to erasure of the thermal history and subsequently cooled to room temperature and heated again. The melting temperatures remained constant at 132°C both in the matrix and in the composites. No change was detected also in the crystallization temperature, which was equal to 114°C in all considered samples. No nucleating effect was therefore observed in nonisothermal conditions. It is known that the nucleating ability of MMT on the crystallization of PE is much dependent on the degree of dispersion of the filler: intercalated clay acts as a retardant, whereas exfoliated clay is a nucleant.[14,23] In our samples, there was not intercalation, and exfoliation was limited to a reduction of tactoid size. This morphology, different from the ideal cases of intercalated and exfoliated nanocomposites, brought about a null effect on nonisothermal crystallization, and thus our samples did not show a shift in T_c. Moreover, Ranade et al.[11] and Liang et al.[4] also pointed out that a large quantity of compatibilizer was necessary to produce heterogeneous nucleation, i.e., 10% of maleated polyethylene. The lower quantities of compatibilizer used in our samples could have prevented the onset of nucleation. Melting and crystallization enthalpies did not display significant variations among the considered samples, confirming WAXD data: the introduction of the filler did not influence the degree of crystallinity of the materials. The effect of MMT on the crystallization kinetics was studied more in depth. It was preliminarily necessary to determine the equilibrium melting temperature (T_m^0) of the samples. This quantity corresponds to the melting temperature of a large stack of perfect extended chain crystals. T_m^0 is very important because, for an accurate study of crystallization kinetics, the supercooling ΔT, i.e., the difference between T_m^0 and the crystallization temperature T_c, must be known. The difference in free energy between melt and crystal phases depends in fact on ΔT, so only comparing polymers crystallized at the same ΔT one can be sure that they experienced the same driving force for crystallization. It is known that the extent of lamellar thickening depends both on T_c and on crystallization time.[35] To rule out the disturbing effect of lamellar thickening, the melting point of initial, nonthickened lamellae (T_m) was estimated. The measurement of this initial T_m was obtained by extrapolation at the induction time, defined as the time when the first deviation of the thermogram baseline is detected. As described in the "Experimental" section, crystallization at each T_c was performed for different times t_c, so that a peak melting temperature vs. log t_c diagram could be plotted and, by linear regression, the extrapolation to t_0 could be calculated.[37] Table II shows the t_0 and

TABLE II
Crystallization Temperatures (T_c), Induction Times (t_0) and Melting Points of Original Lamellae (T_m) of All the Examined Samples

	PE		PE5	
T_c (°C)	t_0 (min)	T_m (°C)	t_0 (min)	T_m (°C)
121	0.7	127	0.7	127
122	2.0	128	2.0	128
123	3.6	129	3.7	129
124	7.4	129	7.4	129

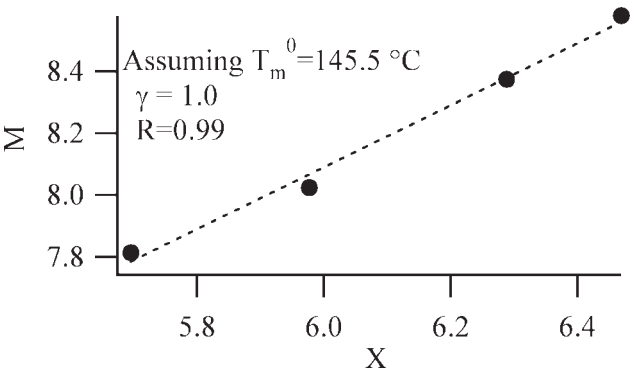

Figure 5 Plot of M vs. X for sample PE, assuming T_m^0= 145.5°C.

the T_m corresponding to each T_c for the base matrix and the nanocomposite containing the highest filler content. It can be seen that t_0 remains constant.

On the basis of the data in Table II, variables M and X were computed as described in the "Experimental" section and for each tentative T_m^0 graphs such as that in Figure 5 were drawn. Each of these datasets was fitted by eq. (4) and the so obtained γ parameter was plotted as a function of T_m^0. Because the melting point of nonthickened lamellae was used in the calculation, the true value of T_m^0 is that for which γ equals to one. Both the matrix and sample PE5 had the same T_m^0 of 145.5°C, in excellent agreement with the values reported in the literature.[22,54] Our HDPE samples behaved differently from other nanocomposites, for example PP-based ones, which usually have lower T_m^0 than their corresponding base polymer.[55–57] The value of T_m^0 of HDPE-based nanocomposites is still controversial. Xu et al.[22] found that an exfoliated HDPE-MMT sample had the same T_m^0 of neat HDPE, whereas in the case of the intercalated material the T_m^0 decreased by 2°C. They invoked the inapplicability of the Hoffman-Weeks extrapolation for the intercalated material because of the small lateral surface of intercalated HDPE crystals. Tanniru et al.,[13] on the other hand, found an increase in the T_m that was interpreted as an increased perfection of the crystals due to the addition of clay particles. The invariability of T_m^0 in our samples is consistent with a limited influence of clay on the structure of the composites.

The isothermal kinetics was quantified by DSC according to the Avrami theory. Table III shows the obtained results. The same values of the n coefficient were obtained for both the matrix and the composites. The mechanism of crystallization was therefore the same both with and without clay. The usual decrease in the kinetic constant k with decreasing ΔT, i.e., with increasing T_c, can be observed in Table III. Moreover, it can be seen that the nanocomposites crystallize at the same rate of the matrix. PLOM confirmed the absence of any nucleating effect. The same spherulitic morphology, characterized by a large quantity of spherulites so tiny that they could not be individually distinguished, even at high magnification, was obtained in all the samples, irrespectively of filler content. This was unexpected, because a nucleating effect has been frequently reported for clay.[3,14,15,23,55,58] The nucleating effect is often associated with the influence of clay on the molecular mobility of the chains.[14,23] To verify this hypothesis, the interfacial free energy σ_e, which is directly proportional to the work of chain folding, was estimated by the Hoffman-Lauritzen theory. This parameter can then be used as a measure for evaluating how easy it is for macromolecules to fold into lamellae. Figure 6 shows the Hoffman-Lauritzen plots obtained for the considered samples. A break in the slope was observed at about 122.5°C (corresponding in Figure 6 to $1/T_c\ \Delta Tf = 110 \times 10^{-6}$), signifying that a change in crystallization regime occurred. This I–II regime transition temperature is lower than the value reported in the literature, i.e, 127°C,[21] probably because of a difference in microstructure between our samples and those employed by the other authors. In this case, it was of interest to study the trend of the I–II transition temperature in the considered samples not its absolute value. The transition between Regimes I and II was observed always at the same temperature for all our samples.

σ_e values (Table IV) could be calculated from the K_g obtained by fitting the lines of Figure 6 by eq. (7). σ_e remains constant in the nanocomposites with

TABLE III
Avrami Parameters for the Considered Samples

	PE		PE05		PE1		PE2		PE5	
ΔT (°C)	n	ln K	n	ln K	n	ln K	n	ln K	n	ln K
27.0	2.0	−0.5	2.1	−0.9	2.0	−0.9	2.0	−0.6	2.2	−0.9
25.0	2.1	−1.9	2.0	−1.7	2.0	−2.1	2.1	−1.9	2.2	−1.8
24.0	2.0	−2.7	2.1	−3.1	2.0	−3.1	2.0	−2.9	2.1	−2.7
23.5			2.1	−4.5	2.2	−4.4	2.2	−4.0	2.3	−4.5
23.0	2.5	−5.7	2.2	−5.4	2.4	−6.1	2.5	−6.1	2.5	−5.9
22.0	2.6	−9.4	2.5	−8.8	2.6	−9.3	2.6	−9.7	2.6	−9.5
21.0	2.7	−12.6							2.8	−13.2

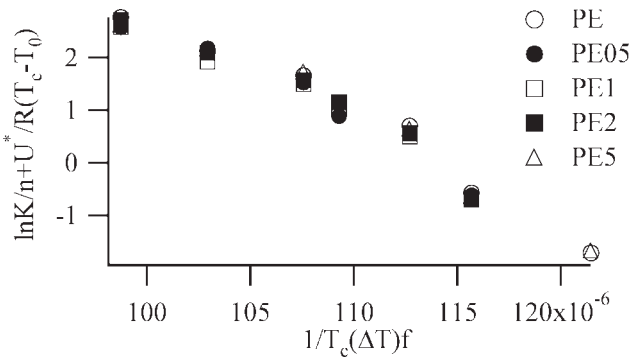

Figure 6 Hoffman-Lauritzen plots for the considered samples.

TABLE IV
Interfacial Free Energies of the Fold Surface for the Considered samples. Superscripts I or II Indicate that the Value was Calculated in the I or II, respectively, Regime of Crystallization

Sample	σ_e^I J·10^5/cm^2	σ_e^{II} J·10^5/cm^2
PE	118	118
PE05	114	114
PE1	116	119
PE2	122	126
PE5	94	115

respect to the base polymer, irrespectively of the regime at which it was calculated. This means that chain folding is neither favored nor hindered in the composites. This explains the absence of nucleation due to clay: the filler did not influence the mobility of the chains, did not act as a nucleation site, and therefore did not alter the rate and the regime of crystallization and the T_m^0 of the samples.

CONCLUSIONS

Nanocomposites based on HDPE and MMT clay were studied, investigating their structure, morphology, thermal behavior, and physical–mechanical properties.

Addition of a filler did not bring about significant structural and morphological modifications with respect to the pristine matrix, with the exception of a disruptive effect on the lamellar stacks and an orientation of crystallites. The crystallization behavior of the nanocomposites was also unaltered with respect to that of the PE-based polymer. Vis-a-vis to these slight changes in the structure and morphology, significant improvements in physical–mechanical properties were observed. This is not a new feature of PE, which shows reinforcement by fillers, without dramatical effects on its structure and morphology.[43] The reason for this increase in performance should therefore be ascribed to the interaction between the filler and the matrix, especially due to a reduction in size of the original tactoids to stacks of just a few layers, albeit not intercalated.

References

1. Ciardelli, F.; Coiai, S.; Passaglia, E.; Pucci, A.; Ruggeri, G. Polym Int 2008, 57, 805.
2. Jeon, H. G.; Jung, H. T.; Lee, S. W.; Hudson, S. D. Polym Bull 1998, 41, 107.
3. Gopakumar, T. G.; Lee, J. A.; Kontopoulou, M.; Parent, J. S. Polymer 2002, 43, 5483.
4. Liang, G. D.; Xu, J. T.; Bao, S. P.; Xu, W. B. J Appl Polym Sci 2004, 91, 3974.
5. Osman, M. A.; Atallah, A. Macromol Rapid Comm 2004, 25, 1540.
6. Osman, M. A.; Rupp, J. E. P.; Suter, U. W. Polymer 2005, 46, 1653.
7. Osman, M. A.; Rupp, J. E. P.; Suter, U. W. Polymer 2005, 46, 8202.
8. Lee, J. H.; Jung, D.; Hong, C. E.; Rhee, K. Y.; Advani, S. G. Compos Sci Tech 2005, 65, 1996.
9. Zhao, C. G.; Qin, H. L.; Gong, F. L.; Feng, M.; Zhang, S. M.; Yang, M. S. Polym Degrad Stab 2005, 87, 183.
10. Modesti, M.; Besco, S.; Lorenzetti, A.; Zanirato, G.; Rauli, F. J Nanosci Nanotech 2005, 5, 958.
11. Ranade, A.; Nayak, K.; Fairbrother, D.; D'souza, N. A. Polymer 2005, 46, 7323.
12. Min, K. D.; Kim, M. Y.; Choi, K. Y.; Lee, J. H.; Lee, S. G. Polym Bull 2006, 57, 101.
13. Tanniru, M.; Yuan, Q.; Misra, R. D. K. Polymer 2006, 47, 2133.
14. Yuan, Q.; Awate, S.; Misra, R. D. K. J Appl Polym Sci 2006, 102, 3809.
15. Chaiko, D. J. e-Polymers 2006, art. no. 019.
16. Mainil, M.; Alexandre, M.; Monteverde, F.; Dubois, P. J Nanosci Nanotech 2006, 6, 337.
17. Deshmane, C.; Yuan, Q.; Perkins, R. S.; Misra, R. D. K. Mater Sci Eng A 2007, 458, 150.
18. Araujo, E. M.; Barbosa, R.; Oliveira, A. D.; Morais, C. R. S.; De Melo, T. J. A.; Souza, A. G. J Therm Anal Calorimetry 2007, 87, 811.
19. Zhong, Y.; Janes, D.; Zheng, Y.; Hetzer, M.; De Kee, D. Polym Eng Sci 2007, 47, 1101.
20. Famulari, A.; Arosio, P.; Filippi, S.; Marazzato, C.; Magagnini, P.; Minkova, L.; Meille, S. V. J Macromol Sci Phys 2007, 46, 355.
21. Xu, J. T.; Zhao, Y. Q.; Fan, Z. Q. Macromol Rapid Comm 2005, 26, 620.
22. Xu, J. T.; Zhao, Y. Q.; Wang, Q.; Fan, Z. Q. Polymer 2005, 46, 11978.
23. Xu, J. T.; Wang, Q.; Fan, Z. Q. Eur Polym J 2005, 41, 3011.
24. Hindeleh, A. M.; Johnson, D. J. J Phys D Appl Phys 1971, 4, 259.
25. Vonk, C. G.; Pijpers, A. P. J Polym Sci Polym Phys 1985, 23, 2517.
26. Vonk, C. G. J Appl Crystallogr 1973, 6, 81.
27. Vonk, C. G. J Appl Crystallogr 1971, 4, 340.
28. Marega, C.; Marigo, A.; Cingano, G.; Zannetti, R.; Paganetto, G. Polymer 1996, 37, 5549.
29. Marega, C.; Marigo, A.; Causin, V. J Appl Polym Sci 2003, 90, 2400.
30. Causin, V.; Marega, C.; Marigo, A.; Ferrara, G. Polymer 2005, 46, 9533.
31. Marega, C.; Causin, V.; Marigo, A. J Appl Polym Sci 2008, 109, 32.

32. Ray, S. S.; Okamoto, M.; Okamoto, M. Macromolecules 2003, 36, 2355.
33. Hosemann, R.; Bagchi, S. N. Direct Analysis of Diffraction by Matter; North Holland Publishing Co.: North Holland, Amsterdam, 1962.
34. Shao, W.; Wang, Q.; Ma, H. Polym Int 2005, 54, 336.
35. Marand, H.; Xu, J.; Srinivas, S. Macromolecules 1998, 31, 8219.
36. Xu, J.; Srinivas, S.; Marand, H.; Agarwal, P. Macromolecules 1998, 31, 8230.
37. Juhász, P.; Varga, J.; Belina, K.; Marand, H. J Therm Anal Calorimetry 2002, 69, 561.
38. Avrami, M. J Chem Phys 1939, 7, 1103.
39. Avrami, M. J Chem Phys 1940, 8, 212.
40. Avrami, M. J Chem Phys 1941, 9, 177.
41. Lauritzen, J. I. J.; Hoffman, J. D. In Treatise on Solid State Chemistry; Hannay, N. B., Ed.; Plenum Press: New York, 1976, Vol. 3, p 497.
42. Truss, R. W.; Yeow, T. K. J Appl Polym Sci 2006, 100, 3044.
43. Causin, V.; Yang, B. X.; Marega, C.; Goh, S. H.; Marigo, A. J Nanosci Nanotech 2008, 8, 1790.
44. Lincoln, D. M.; Vaia, R. A.; Wang, Z.; Hsiao, B. S.; Krishnamoorti, R. Polymer 2001, 42, 9975.
45. Maiti, P.; Nam, P. H.; Okamoto, M.; Hasegawa, N.; Usuki, A. Macromolecules 2002, 35, 2042.
46. Causin, V.; Marega, C.; Marigo, A.; Ferrara, G.; Ferraro, A.; Selleri, R. J Nanosci Nanotech 2008, 8, 1823.
47. Causin, V.; Carraro, M. L.; Marega, C.; Saini, R.; Campestrini, S.; Marigo, A. J Appl Polym Sci 2008, 109, 2354.
48. Truss, R. W.; Lee, A. C. Polym Int 2003, 52, 1790.
49. Zhang, J. G.; Wilkie, C. A. Polymer 2006, 47, 5736.
50. Qin, H.; Zhang, S.; Zhao, C.; Yang, M. J Polym Sci Polym Phys 2005, 43, 3713.
51. Mishra, J. K.; Hwang, K.-J.; Ha, C.-S. Polymer 2005, 46, 1995.
52. Lee, H.; Fasulo, P. D.; Rodgers, W. R.; Paul, D. R. Polymer 2005, 46, 11673.
53. Lomakin, S. M.; Dubnikova, I. L.; Shchegolikhin, A. N.; Zaikov, G. E.; Kozlowski, R.; Kim, G. M.; Michler, G. H. J Therm Anal Calorimetry 2008, 94, 719.
54. Keum, J. K.; Somani, R. H.; Zuo, F.; Burger, C.; Sics, I.; Hsiao, B. S.; Chen, H.; Kolb, R.; Lue, C. T. Macromolecules 2005, 38, 5128.
55. Causin, V.; Marega, C.; Saini, R.; Marigo, A.; Ferrara, G. J Therm Anal Calorimetry 2007, 90, 849.
56. Arroyo, M.; Lopez-Manchado, M. A.; Avalos, F. Polymer 1997, 38, 5587.
57. Varma-Nair, M.; Agarwal, P. K. J Therm Anal Calorimetry 2000, 59, 483.
58. Leszczynska, A.; Pielichowski, K. J Therm Anal Calorimetry 2008, 93, 677.